MOLECULAR CARCINOGENESIS 53:159–167 (2014)

BRIEF COMMUNICATION

A Subset of Papillary Thyroid Carcinomas Contain *KRAS* Mutant Subpopulations at Levels Above Normal Thyroid

Meagan B. Myers,* Karen L. McKim, and Barbara L. Parsons

Division of Genetic and Molecular Toxicology, National Center for Toxicological Research, U.S. Food and Drug Administration, Jefferson, Arkansas

The molecular pathogenesis of papillary thyroid carcinoma (PTC) is largely attributed to chromosomal rearrangements and point mutations in genes within the MAPK pathway (i.e., *BRAF* and *RAS*). Despite *KRAS* being the 6th most frequently mutated gene for all cancers, the reported frequency in thyroid cancer is only 2%. This may be due, in part, to the use of insensitive mutation detection methods such as DNA sequencing. Therefore, using the sensitive and quantitative ACB-PCR approach, we quantified *KRAS* codon 12 GGT → GAT and GGT → GTT mutant fraction (MF) in 20 normal thyroid tissues, 17 primary PTC, 2 metastatic PTC, and 1 anaplastic thyroid carcinoma. We observed measurable levels of *KRAS* codon 12 GAT or GTT mutation in all normal thyroid tissues. For PTCs, 29.4% and 35.3% had *KRAS* codon 12 GAT and GTT MF above the 95% upper confidence interval for the corresponding MFs in normal thyroid. The highest observed *KRAS* codon 12 GTT MFs were associated with tumors with follicular characteristics and relatively high levels of tumor necrosis. The results indicate *KRAS* mutant subpopulations are present in a large number of thyroid tumors, a fact previously unrecognized. The presence of *KRAS* mutation may indicate a tumor with an aggressive phenotype, thus directing the course of clinical treatment.

Key words: ACB-PCR; cancer biomarkers; cancer genetics; mutation; oncogenes

INTRODUCTION

The incidence of thyroid cancer, the most prevalent endocrine malignancy, has nearly tripled since the mid-1970s. This is largely attributed to access of improved detection methodologies (ultrasonography and fine needle aspiration) and changes in diagnostic criteria [1,2]. It is unclear how much other factors, that is, environmental, contribute to this increase. Exposure to ionizing radiation is a well-documented risk factor [3], while exposure to organochlorinated pollutants [4] or high levels of iodine and other chemicals in drinking water [5] have been suggested as risk factors. Notably, an increased incidence of thyroid cancer, along with soft-tissue sarcoma and brain cancer, was reported in men from a Spanish community chronically exposed to high levels of hexachlorobenzene [4]. Persistent organochlorinated pollutants such as hexachlorobenzene are highly lipophilic, and thus, concentrate in fat and lipid-bearing tissues, such as thyroid [6].

Papillary thyroid cancer (PTC) accounts for approximately 80–90% of all thyroid cancers. Although the majority of these tumors behave in an indolent fashion, which infers favorable prognosis, a subset of these tumors behave aggressively and result in poor clinical outcome. Mutations within genes of the MAPK pathway are common in PTC and are thought to be essential in the initiation of tumorigenesis [7,8]. The type and frequencies of these mutations depend on the subtype of PTC, with point mutations in *BRAF* occurring more often in the classic and tall-cell variants, while mutations in *RAS* are thought to be found almost exclusively in follicular variant of PTC [9]. While *KRAS* is the predominate *RAS* mutation in most types of cancer, in thyroid cancer, *NRAS* is reported to be the most prevalent *RAS* mutation [10]. Mutations in *RAS* appear to define a subset of thyroid carcinomas with aggressive behavior and poor survival outcomes [11,12]. Indeed, *RAS* mutations are one of the most prevalent molecular alterations in poorly differentiated thyroid carcinomas (PDTC) [12–14]. They occur with higher frequencies in these tumors than in well differentiated PTC, implicating *RAS* in the progression and aggressiveness of this tumor type

Abbreviations: PTC, papillary thyroid carcinoma; ACB-PCR, allele-specific competitive blocker polymerase chain reaction; NDRI, National Disease Research Interchange; CHTN, Cooperative Human Tissue Network; ATC, anaplastic thyroid carcinoma; MF, mutant fraction; LNM, lymph node metastasis;.

*Correspondence to: Division of Genetic and Molecular Toxicology, HFT-120, 3900, NCTR Road, Jefferson, AR 72079.

Received 29 March 2012; Revised 27 July 2012; Accepted 1 August 2012

DOI 10.1002/mc.21953

Published online 28 August 2012 in Wiley Online Library (wileyonlinelibrary.com).

[12,13]. Despite the role of *RAS* mutation in the pathogenesis of thyroid cancer, its potential as a biomarker of aggressive disease has not been rigorously investigated.

As part of a broad project to establish specific hotspot oncomutations as quantitative biomarkers of cancer risk, we are quantifying levels of particular activating mutations in normal human tissues and in the tumors that arise in them. To accomplish this, we are employing allele-specific competitive blocker PCR (ACB-PCR), a sensitive and quantitative method for the characterization of low frequency hotspot point mutations (i.e., at ratios as low as one mutant DNA sequence per 100,000 wild-type DNA sequences) [15–19]. Using the ACB-PCR method, we previously showed that *KRAS* mutation is often present as a mutant tumor subpopulation in colon tumors, at levels not detectable by DNA sequencing [17]. In the current study, we utilized the ACB-PCR approach to quantify *KRAS* codon 12 GGT → GAT and GGT → GTT mutation in 20 normal thyroid tissues and 20 thyroid tumors surgically removed from cancer patients. Herein, we report that a subset of PTCs possess *KRAS* mutant subpopulations at levels above those found in normal thyroid tissues.

MATERIALS AND METHODS

Normal Thyroid and Tumor Samples

This study, involving collection of anonymous human tissues, was reviewed by the FDA Research Involving Human Subjects Committee (RIHSC, FWA 00006196). Twenty fresh-frozen normal thyroid samples, collected at the time of autopsy, were purchased from the National Disease Research Interchange (NDRI; Philadelphia, PA). Eighteen fresh-frozen PTCs were provided by the National Cancer Institute-Cooperative Human Tissue Network [NCI-CHTN; including 7 PTCs from the Southern Division (University of Alabama at Birmingham, Birmingham, AL), 10 PTCs from the Mid-Atlantic Division (University of Virginia, Charlottesville, VA), and 1 PTC from the Western Division (Vanderbilt University Medical Center, Nashville, TN)]. One PTC was purchased from NDRI. In addition, one anaplastic thyroid carcinoma (ATC) was purchased from NDRI. All tumor specimens were histologically evaluated by board certified pathologists to confirm the original diagnosis.

DNA Isolation

DNAs from normal thyroid and thyroid tumors were isolated, employing precautions to limit the possibility of cross-contamination. Tissues were homogenized using an Omni THQ tissue homogenizer (Omni International, Kennesaw, GA) and 6 ml of proteinase K buffer [1 mg/ml proteinase K, 100 mM NaCl, 2.5 mM EDTA (pH 8), and 0.1% SDS] per gram of tissue, incubated ~16 h at 37°C, and then extracted with an equal volume of a 25:24:1 phenol/chloroform/isoamyl alcohol mixture. Samples were resuspended in 200 μl of RNase buffer: 10 mg/ml RNase A (Sigma, St. Louis, MO), 4.2 units/μl ribonuclease T1 (Sigma), 100 mM sodium acetate, and 50 mM Tris–HCl (pH 8), incubated ~16 h at 37°C, and extracted as described above. The DNA was precipitated with ethanol and resuspended in TE buffer (5 mM Tris, 0.5 mM EDTA, pH 7.5). All genomic DNAs were restriction digested, phenol/chloroform/isoamyl alcohol extracted, ethanol-precipitated, and resuspended in TE buffer to a final concentration of ~500 ng/μl.

First-Round PCR

High-fidelity, first-round PCR reactions were performed using 1 μg of digested normal thyroid or thyroid tumor genomic DNA as template. The 200 μl PCR reaction contained: 10 mM KCl, 10 mM $(NH_4)_2SO_4$, 20 mM Tris–HCl (pH 8.75), 2 mM $MgSO_4$, 0.1% Triton X–100, 0.1 mg/ml bovine serum albumin, 0.2 mM dNTPs, 0.2 μM RD1 (5′TTAAGCGTCGATGGAGGAGTT-3′), 0.2 μM RD2 (5′-GTCCTGCACCAGTAATATGC-3′), and 4 units of cloned *PfuUltra* Hotstart DNA Polymerase (Stratagene, La Jolla, CA). The first-round PCR included a 2 min denaturation at 94°C, followed by 35 cycles of 1 min at 94°C, 1 min at 56°C, and 1 min at 72°C, and a final 7 min extension at 72°C. The 384 bp *KRAS* PCR product (which included sequence 5′ of exon 1, exon 1, and part of intron 1) was isolated following preparative agarose gel electrophoresis using a Geneclean Spin Kit (MP Biomedicals, Solon, OH) and frozen as multiple single-use aliquots. The concentration of each DNA sample was determined by repeated measurement using an Epoch Spectrophotometer (BioTek, Winooski, VT); final concentrations were calculated once three determinations that varied by ≤10% from the group mean were obtained.

ACB-PCR

ACB-PCR quantification relies upon parallel analyses of a set of mutant fraction (MF) standards and first-round PCR products generated from unknown samples, all of which contain equal numbers of *KRAS* molecules. Mutant and wild-type standards were prepared by digestion of cloned mutant or wild-type plasmid DNA (wild-type, codon 12 GGT; A mutant, codon 12 GAT; and T mutant, codon 12 GTT) with Afl II and Ava II and isolation of a DNA segment identical in sequence composition to the first-round PCR product prepared from isolated thyroid DNA samples.

Purified mutant and wild-type reference DNAs were mixed to generate standards with MFs of 10^{-1}, 10^{-2}, 10^{-3}, 10^{-4}, 10^{-5}, and 0 (containing only the wild-type *KRAS* codon 12 sequence), at a concentration of 5×10^7 copies/μl. These standards were

analyzed in parallel with equal numbers of copies of unknown first-round PCR products. Each ACB-PCR reaction incorporated 10 μl of each DNA mixture, for a total of 5×10^8 *KRAS* copies per reaction. Each MF standard was analyzed in duplicate, along with a no-DNA control. The ACB-PCR was performed in a 96-well PCR plate (Thermo Fisher Scientific, Waltham, MA) using a DNA Engine thermal cycler (Bio-Rad, Hercules, CA). For measurement of *KRAS* codon 12 GAT MF by ACB-PCR, each 50 μl reaction contained: 1× Stoffel buffer (10 mM KCl, 10 mM Tris–HCl, pH 8.3), 1.6 mM $MgCl_2$, 0.1 mg/ml gelatin, 1.0 mg/ml Triton X-100, 80 μM dNTPs, 20 mU PerfectMatch PCR Enhancer (Agilent Technologies, Santa Clara, CA), 500 nM primer P4 (5′-GATTTACCTCTATTGTTGGA-3′), 500 nM MSP-A (5′-fluorescein-CTTGTGGTAGTTGGAGCTTA-3′), and 475 nM BP-A (5′-CTTGTGGTAGTTGGAGCTTdG -3′). For measurement of *KRAS* codon 12 GTT MF by ACB-PCR, each 50 μl reaction contained: 1× Stoffel buffer, 1.5 mM $MgCl_2$, 0.1 mg/ml gelatin, 1.0 mg/ml Triton X-100, 40 μM dNTPs, 90 mU PerfectMatch PCR Enhancer, 400 nM primer P3 (5′-GTTGGATCATATTCGTCCAC-3′), 400 nM MSP-T (5′-fluorescein-CTTGTGGTAGTTGGAGCTAT-3′), and 400 nM BP-T (5′-CTTGTGGTAGTTGGAGCTAdG-3′). Each reaction was started with the addition of 3.33 U of a hotstart formulation of Stoffel DNA polymerase, which was prepared by incubating *Taq* DNA polymerase Stoffel fragment (Life Technologies, Grand Island, NY) with Platinum *Taq* antibody (Life Technologies) at a 1:1 unit ratio for 30 min on ice. Cycling conditions for the *KRAS* GAT ACB-PCR were 36 cycles of 30 s at 94°C, 45 s at 45°C, and 1 min at 72°C. Cycling conditions for the *KRAS* GTT ACB-PCR were 36 cycles of 30 s at 94°C, 45 s at 41°C, and 1 min at 72°C.

Gel Electrophoresis, Image Analysis, and Data Collection

Each ACB-PCR product was analyzed on non-denaturing 8% polyacrylamide gels. The fluorescent bands were visualized using a PharosFX Molecular Imager with an external blue laser (Bio-Rad). Pixel intensities of the bands (GAT ACB-PCR, 103 bp; GTT ACB-PCR, 89 bp) were quantified using Quantity One software and a locally averaged background correction (Bio-Rad). Log-linear plots relating MF to fluorescence (in pixels) were constructed and fit with an exponential function. This function was then used to calculate the MF in each unknown sample based on the fluorescence of the ACB-PCR product generated using that sample and the same quantitation methodology.

Statistical Analyses

The *KRAS* MF for each sample was calculated as the arithmetic average of three independent MF measurements. The average MF measurement for each sample was $\log_{10}$-transformed. The average of the $\log_{10}$-transformed MF measurements was calculated then converted back to scientific notation to obtain the geometric mean (geomean) MF for each group. Log_{10}-transformed data were used for statistical analyses. Comparison between two groups was performed using Student's *t*-test for normally distributed variables and Mann–Whitney rank sum test for non-normally distributed variables. One-way ANOVA (Kruskal–Wallis), followed by the Dunn's Multiple Comparison Test, was performed on groups of 3 or more. Correlation analysis was performed on available data using the Spearman's rank order correlation coefficient test. Two-tailed *P* values of <0.05 were considered significant. All statistical analysis was performed using GraphPad Prism Software (GraphPad Software, Inc., La Jolla, CA).

RESULTS AND DISCUSSION

The *KRAS* codon 12 GAT and GTT MFs in 20 normal thyroid tissue samples and in 20 thyroid tumors [(17 primary PTC, 2 metastatic PTCs (mPTC), and 1 ATC] were measured by ACB-PCR. The average MF and SD for each MF measurement (3 independent experiments, except for sample #12, with only 2 GAT measurements) are plotted in Figure 1.

The normal thyroid samples included 10 males and 10 females aged 32–84 yrs old (61.30 ± 15.87 yrs old, mean ± SD). Every normal thyroid sample had a measurable level of either *KRAS* codon 12 GAT or GTT mutation, with 19/20 and 15/20 samples having MF levels $\geq 10^{-5}$ for the GAT or GTT mutation, respectively. The *KRAS* codon 12 GAT and GTT geometric mean MFs for normal thyroid were 1.72×10^{-5} and 1.31×10^{-5}, respectively. Levels of *KRAS* codon 12 GAT mutation were significantly higher than the levels of *KRAS* codon 12 GTT mutation (two-tailed, Mann–Whitney rank sum test; $P = 0.0155$). This is consistent with previous findings in other tissues [17]. This may be explained by removal of cells displaying the more aberrant GTT activating phenotype through tissue homeostatic mechanisms [20,21].

In total, 20 thyroid tumors (17 primary PTCs, 2 mPTCs, and 1 ATC) were measured for *KRAS* codon 12 GAT and GTT mutations by ACB-PCR. A summary of the pathological and clinical features of each thyroid tumor and its corresponding *KRAS* codon 12 GAT and GTT MF is given in Table 1. Only data obtained from primary PTCs were considered in the statistical analyses. According to the Catalogue of Somatic Mutations in Cancer (COSMIC) database, only 0.63% and 0.16% of PTC samples are positive for the *KRAS* codon 12 GAT or GTT mutation, respectively [6]. However, using the sensitive ACB-PCR approach, we found 15/17 and 10/17 tumors had *KRAS* codon 12 GAT or GTT MFs $\geq 10^{-5}$, respectively. This demonstrates that *KRAS* mutations are often present at levels that would be missed by less sensitive approaches, such as DNA sequencing or

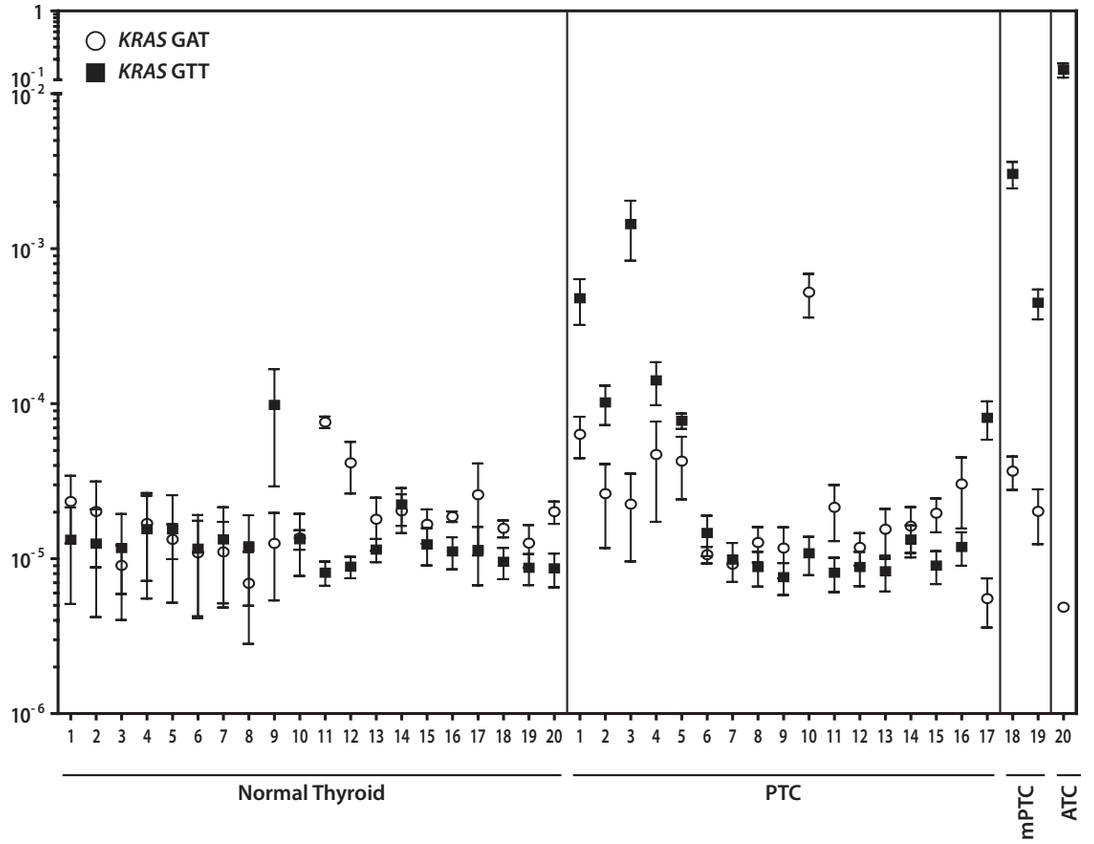

Figure 1. *KRAS* codon 12 MF measurements for each normal thyroid and thyroid tumor sample. Open circles denote the mean *KRAS* codon 12 GAT MF calculated from three replicate experiments and the black squares denote the mean *KRAS* codon 12 GTT MF. Error bars indicate SD for mean *KRAS* codon 12 MFs in normal thyroid ($n = 20$), papillary thyroid carcinomas (PTC; $n = 17$), metastatic papillary thyroid carcinomas (mPTC; $n = 2$), and anaplastic thyroid carcinoma (ATC; $n = 1$). For the PTCs, samples 1–5 are from CHTN-Southern Division, 6–15 are from CHTN-Mid Atlantic Division, sample 16 is from CHTN-Western Division, and sample 17 is from NDRI.

even quantitative real-time PCR. The *KRAS* codon 12 GAT and GTT geometric mean MFs for all primary PTCs were 2.28×10^{-5} and 2.85×10^{-5}, respectively, which were not significantly different from normal thyroid (two-tailed, Mann–Whitney rank sum test; $P = 0.72$ and $P = 0.80$, GAT and GTT, respectively). However, a number of thyroid tumor samples had relatively high *KRAS* MFs, as compared to the normal tissue samples (Figure 1). 29.4% and 35.3% of primary PTCs had *KRAS* codon 12 GAT and GTT MF above the upper 95% confidence interval for the corresponding MFs in normal thyroid tissue. Thus, a significant number of thyroid tumors carry *KRAS* mutation above the level found in normal thyroid tissues, as a subpopulation of tumor cells. These data indicate that *KRAS* mutation may play a larger role than previously realized in the etiology of a subset of PTCs. In addition, the presence of relatively high *KRAS* GTT MF in the lymph node metastases (LNM) of two patients, and in the ATC (*KRAS* GTT MF of 1.40×10^{-1}) further implicates *KRAS* in the pathogenesis of thyroid cancer.

Interestingly, we observed an apparent difference in *KRAS* codon 12 GTT MF relative to tumor source (with samples obtained from the Southern Division of the CHTN having a higher MF than those from the Mid-Atlantic Division; Table 1 and Figure 2). Comparing *KRAS* codon 12 GAT and GTT MFs in normal thyroid samples to that of primary PTCs stratified by tumor source showed significant differences in the median *KRAS* codon 12 GAT and GTT MFs (Kruskal–Wallis; $P = 0.015$ and $P = 0.0015$, GAT and GTT, respectively). Post-test analysis (Dunn's Multiple Comparison Test) indicated the *KRAS* GTT MF was significantly higher in primary PTCs from the Southern Division of the CHTN than in normal thyroid samples ($P < 0.05$) or PTCs from the Mid-Atlantic Division of the CHTN ($P < 0.001$; Figure 2).

Multiple characteristics of the primary PTC samples were examined in order to identify an underlying bias that could explain the distribution of *KRAS* MFs relative to tumor source (Table 2). Despite our relatively low sample numbers, some significant

Table 1. Pathological and Clinical Features of Thyroid Tumors and Their Corresponding *KRAS* Codon 12 GAT and GTT Mutant Fractions

Tumor type	Supplier	ID	Sex/age	Stage; annotated pathological features	Multifocal	% Tumor	% Necrosis	Max. dimension[a]	Thyroid encap.	LNM	KRAS GAT		KRAS GTT	
											MF	Geomean	MF	Geomean
Primary PTC	CHTN-Southern	1	F/31	Stage I; conventional type	Y	80	0	1.4	N	Y	6.34×10^{-5}	3.76×10^{-5}	4.79×10^{-4}	2.34×10^{-4}
		2	M/45	Stage IVA	N	80	0	2.0	N	Y	2.62×10^{-5}		1.02×10^{-4}	
		3[b]	M/33	Stage I; papillary and follicular features	N	100	20	2.2	N	Y	2.25×10^{-5}		1.44×10^{-3}	
		4	M/41	Stage I; follicular pattern	Y	70	60	1.6	N	Y	4.69×10^{-5}		1.41×10^{-4}	
		5	F/69	Stage III; follicular variant	N	80	0	2.8	N		4.26×10^{-5}		7.75×10^{-5}	
	CHTN-Mid Atlantic	6	F/19	Stage I; tall cell variant	N	80	0	6.7	N	Y	1.06×10^{-5}	1.98×10^{-5}	1.46×10^{-5}	9.71×10^{-6}
		7	F/63	Stage III	Y	90	0	2.5		Y	9.20×10^{-6}		9.85×10^{-6}	
		8	F/74	Stage III	N	100	0	4.1		Y	1.27×10^{-5}		8.83×10^{-6}	
		9	M/66	Stage IVA	Y	90	0	3.5	N	Y	1.17×10^{-5}		7.59×10^{-6}	
		10	F/86	Stage III; evidence of hashimoto's/thyroiditis	Y	100	0	4.5	Y	N	5.23×10^{-4}		1.08×10^{-5}	
		11	M/30	Stage I	N	100	0	6.5		Y	2.14×10^{-5}		8.11×10^{-6}	
		12	F/71	Stage IVA	Y	100	0	3.5	N	Y	1.18×10^{-5}		8.84×10^{-6}	
		13	F/28	Stage I; classic	N	100	0	1.5	Y	N	1.55×10^{-5}		8.28×10^{-6}	
		14	F/24	Stage I	N	100	0	2.8	Y	Y	1.62×10^{-5}		1.33×10^{-5}	
		15	M/30	Stage I	N	75	0	3.2	Y	Y	1.96×10^{-5}		9.02×10^{-6}	
	CHTN-Western	16	M/23	Stage I; some columnar histology	Y	90	0	7.0	Y	N	3.03×10^{-5}	—	1.19×10^{-5}	—
	NDRI	17	M/41	Stage I	Y	100	0	2.3	N	Y	5.52×10^{-6}	—	8.09×10^{-5}	—
mPTC/right neck mass	CHTN-Southern	18[b]	M/33	Stage I; cystic, classic and follicular growth patterns	—	100	40	2.2	na	na	2.02×10^{-5}		4.48×10^{-4}	
mPTC to the lymph	CHTN-Southern	19[c]	M/74	Stage IVA	—	70	0	4.5	na	na	3.66×10^{-5}	—	3.04×10^{-3}	—
ATC	NDRI	20	F/68	Stage IVA	—	100	0	6.5	N	Y	4.86×10^{-6}	—	1.40×10^{-1}	—

ATC, anaplastic thyroid carcinoma; CHTN, Cooperative Human Tissue Network, geomean, geometric mean; LNM, lymph node metastasis, MF, mutant fraction; mPTC, metastatic papillary thyroid carcinoma, NDRI, National Disease Research Interchange; PTC, papillary thyroid carcinoma, Thyroid encap., thyroid encapsulated.

[a]In centimeters.

[b]Samples are from same patient; right neck mass was removed 1 month prior to thyroid and lymph node dissection.

[c]Sample from patient with history of thyroid cancer (15 yrs prior).

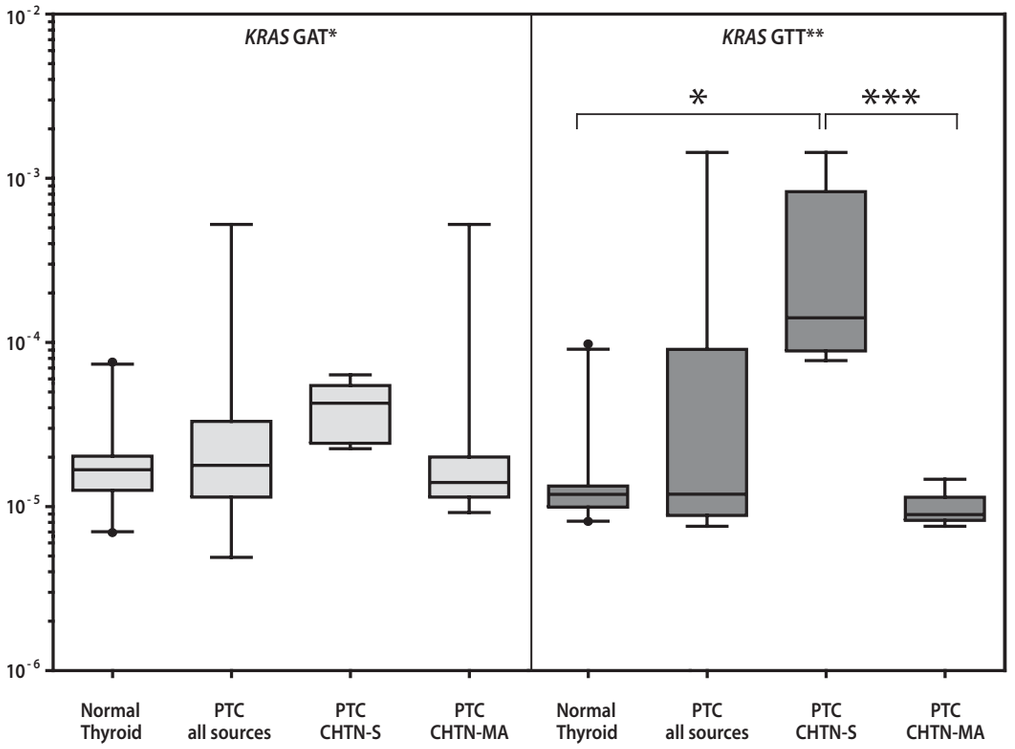

Figure 2. Box and whisker plots describing the distribution of *KRAS* codon 12 GAT (light gray) and GTT (dark gray) MF measurements in normal thyroid and primary papillary thyroid carcinoma (PTC) according to source. The horizontal line indicates the median MF, the boxes indicate the 25th and 75th percentiles, error bars indicate the 5th and 95th percentiles. Asterisks indicate significance ($^{*}P \leq 0.05$, $^{**}P \leq 0.01$, $^{***}P \leq 0.001$).

correlations were found. Increased *KRAS* GTT MF was associated with the presence of follicular characteristics ($r = 0.54$, $P = 0.0268$) and higher percent necrosis ($r = 0.53$, $P = 0.0361$), which were found to exist only in samples from the Southern Division of the CHTN. Indeed, *RAS* mutations (mostly *NRAS* and *HRAS*) are thought to be found almost exclusively in follicular adenomas/carcinomas, or in the follicular variant of PTC (FVPTC), and are generally associated with low rate of LNM and the lack of extrathyroidal extension [9]. Contrary to what has been described in the literature, our three primary PTCs with follicular characteristics had the highest measured *KRAS* codon 12 GTT MFs, in addition to the presence of extrathyroidal extension and LNM. The reason for this discrepancy is not clear, however, two of our three primary PTCs with follicular characteristics contained high percentages of necrosis, which could indicate that these tumors are, in fact, poorly differentiated thyroid carcinomas (PDTC) [22]. Thyroid tumors classified as PDTC by the extent of necrosis and/or mitosis (regardless of growth pattern and cell type) lead to radioactive iodine refractory (RAIR), positron emission topography-positive incurable carcinoma, and have decreased overall survival [22,23]. These tumors have been shown to have high frequencies of *N-/H-/K-RAS* mutation [12–14], consistent with the observations in this study. Furthermore, oncogenic *KRAS* was shown to correlate independently with loss of tumor differentiation and distant metastasis, indicating *KRAS* as a marker for thyroid tumor aggressiveness [11]. Finally, *KRAS* GTT MF was inversely associated with maximum dimension of the tumor ($r = -0.51$, $P = 0.0418$), which was significantly lower in samples obtained from the Southern Division compared to the Mid-Atlantic Division of the CHTN (two-tailed *t*-test; $P = 0.03$). Collectively, these associations may explain the higher *KRAS* GTT MF in the PTCs from the Southern Division of the CHTN.

Other correlative observations include the association of multifocality of the PTC (presence in multiple lobes of the thyroid) and male patients ($r = 0.53$, $P = 0.0294$) and maximum dimension of tumor ($r = 0.52$, $P = 0.0332$). The lack of confinement of the primary PTC to the thyroid was correlated with LNM ($r = -0.59$, $P = 0.0332$). Age and tumor stage were also associated ($r = 0.80$, $P = 0.0001$); however, this is likely a function of the American Joint Committee on Cancer thyroid staging guidelines, in which all thyroid cancer patients

Table 2. Spearman's Rank Order Correlation Coefficients (ρ) of 13 Parameters in Primary Papillary Thyroid Carcinomas

Variable	Mean (SD) or fraction of samples	Source	*KRAS* GTT	*KRAS* GAT	Age	Sex	Stage	Multi focal	Thyroid encap.	LNM	Max. dim.	% Tumor	% Necrosis	FC
Source (1 = CHTN-S, 2 = CHTN-MA, 3 = CHTN-W, 4 = NDRI)	0.29 CHTN-S, 0.59 CHTN-MA, 0.06 CHTN-W, 0.06 NDRI	—	−0.72***	−0.19	−0.22	−0.21	0.06	0.21	0.39	−0.46	0.70**	0.22	−0.42	−0.54*
KRAS GTT	2.85×10^{-5}[a]		—	0.41	−0.13	0.12	−0.30	−0.22	−0.39	0.19	−0.50*	−0.36	0.52*	0.54*
KRAS GAT	2.28×10^{-5}[a]			—	0.06	0.07	−0.12	−0.36	−0.07	−0.36	−0.16	−0.29	0.31	0.41
Age	45.5 (21.3)				—	−0.19	0.80*	−0.28	−0.30	0.12	−0.02	0.16	−0.02	0.14
Sex (0 = female, 1 = male)	0.47 male					—	−0.19	0.53*	0.00	0.16	−0.01	−0.21	0.39	0.18
Stage (1 = Stage I, 2 = Stage II, 3 = Stage III, 4 = Stage IV)	0.59 Stage I, 0.23 Stage III, 0.18 Stage IV						—	−0.29	−0.40	0.10	0.13	0.04	−0.29	−0.12
Multifocal (0 = no, 1 = yes)	0.47 multifocal							—	0.13	0.16	0.52*	0.12	0.00	−0.13
Thyroid encapsulated (0 = no, 1 = yes)	0.30 encapsulated								—	−0.59*	0.20	0.40	−0.35	−0.45
LNM (0 = no, 1 = yes)	0.77 LNM									—	−0.19	−0.24	0.18	0.18
Max. dimension	3.42 (1.81)										—	0.20	−0.38	−0.33
% Tumor	0.90 (0.11)											—	−0.17	−0.27
% Necrosis	0.05 (0.16)												—	0.79***
Follicular characteristics (0 = no, 1 = yes)	0.24 FC													—

CHTN, Cooperative Human Tissue Network; CHTN-M, CHTN-Mid-Atlantic Division; CHTN-S, CHTN-Southern Division; CHTN-W, CHTN Western Division; FC, follicular characteristics; LNM, lymph node metastasis; NDRI, National Disease Research Interchange, Thyroid encap., thyroid encapsulated.

*$P \leq 0.05$.

**$P \leq 0.01$.

***$P \leq 0.001$.

[a]Geometric mean.

<45 yrs old that do not present with distant metastasis are classified as Stage I.

In summary, using the ACB-PCR method, we show that *KRAS* mutation is present in a surprisingly high number of thyroid tumors, but as a minor subpopulation. It is unclear what clinical impact these minor *KRAS* mutant subpopulations may have. Evidence is accumulating that mutant subpopulations (too small to be detectable by DNA sequencing) may contribute to resistance/relapse following molecularly targeted treatment [24–26]. In thyroid cancer, upregulation of epidermal growth factor receptor (EGFR) protein expression is associated with the progression of well differentiated thyroid carcinomas to poorly differentiated and anaplastic thyroid carcinomas [27], suggesting EGFR as a potential therapeutic target for these aggressive tumors. However, one phase II study of the EGFR tyrosine kinase inhibitor gefitinib found no partial or complete response in patients with advanced thyroid cancer [28]. This study failed to analyze tumors for the presence of *KRAS* mutation, which is an established molecular biomarker of resistance to EGFR-targeted therapies [29]. It is possible that *KRAS* mutant subpopulations, like those identified in this study, could help explain the lack of response, in at least some patients. Moreover, any therapy that targets signaling molecules upstream of *KRAS* may result in the outgrowth of *KRAS* mutant subpopulations and lead to relapse, as has been shown for lung and colon cancer [29].

Lastly, the high prevalence of *BRAF* mutation in thyroid cancer, along with the positive results seen with selective BRAF inhibitors in melanoma patients, has brought about several clinical trials utilizing these inhibitors in thyroid cancer patients (http://www.clinicaltrials.gov). However, it has recently been established that in the presence of mutated or activated *RAS*, BRAF inhibition leads to the paradoxical induction of the RAS-RAF-ERK pathway, resulting in cell proliferation both in vitro and in vivo [30–33]. In addition, it has been confirmed that *RAS* mutations are associated with the development of keratoacanthomas and cutaneous squamous cell carcinomas after treatment with the BRAF inhibitors, vemurafenib or sorafenib [34–36]. Consequently, the potential implications of *KRAS* mutant subpopulations should be considered when using BRAF inhibitors in thyroid cancer patients whose tumors have not been analyzed for the presence of *KRAS* using a sensitive method. Not only is there potential for *KRAS* mutant subpopulations to impact patient response and relapse, but to also impact the outcome of the clinical trial itself.

ACKNOWLEDGMENTS

The authors thank Drs. James Fuscoe and Deborah Hanson for their critical review of this manuscript. Tissue samples were provided by the Cooperative Human Tissue Network, a National Cancer Institute supported resource. Other investigators may have received samples from these same tissue specimens. We acknowledge use of tissues procured by the National Disease Research Interchange (NDRI; with support from NIH grant 5 U42 RR006042). The contents of this manuscript do not necessarily reflect the views or policies of the U.S. Food & Drug Administration, nor does the mention of trade names or commercial products constitute endorsement or recommendation for use. This study was supported by National Center for Toxicological Research and U.S. Food & Drug Administration.

REFERENCES

1. Albores-Saavedra J, Henson DE, Glazer E, Schwartz AM. Changing patterns in the incidence and survival of thyroid cancer with follicular phenotype–papillary, follicular, and anaplastic: A morphological and epidemiological study. Endocr Pathol 2007;18:1–7.
2. Davies L, Welch HG. Increasing incidence of thyroid cancer in the United States, 1973–2002. JAMA 2006;295:2164–2167.
3. Ron E, Lubin JH, Shore RE, et al. Thyroid cancer after exposure to external radiation: A pooled analysis of seven studies. Radiat Res 1995;141:259–277.
4. Grimalt JO, Sunyer J, Moreno V, et al. Risk excess of soft-tissue sarcoma and thyroid cancer in a community exposed to airborne organochlorinated compound mixtures with a high hexachlorobenzene content. Int J Cancer 1994;56:200–203.
5. Nikiforov YE, Nikiforova MN. Molecular genetics and diagnosis of thyroid cancer. Nat Rev Endocrinol 2011;7:569–580.
6. Langer P. Persistent organochlorinated pollutants (PCB, DDE, HCB, dioxins, furans) and the thyroid—Review 2008. Endocr Regul 2008;42:79–104.
7. Kimura ET, Nikiforova MN, Zhu Z, Knauf JA, Nikiforov YE, Fagin JA. High prevalence of BRAF mutations in thyroid cancer: Genetic evidence for constitutive activation of the RET/PTC-RAS-BRAF signaling pathway in papillary thyroid carcinoma. Cancer Res 2003;63:1454–1457.
8. Soares P, Trovisco V, Rocha AS, et al. BRAF mutations and RET/PTC rearrangements are alternative events in the etiopathogenesis of PTC. Oncogene 2003;22:4578–4580.
9. Adeniran AJ, Zhu Z, Gandhi M, et al. Correlation between genetic alterations and microscopic features, clinical manifestations, and prognostic characteristics of thyroid papillary carcinomas. Am J Surg Pathol 2006;30:216–222.
10. COSMIC Database. http://www.sanger.ac.uk/genetics/CGP/cosmic
11. Garcia-Rostan G, Zhao H, Camp RL, et al. ras mutations are associated with aggressive tumor phenotypes and poor prognosis in thyroid cancer. J Clin Oncol 2003;21:3226–3235.
12. Volante M, Rapa I, Gandhi M, et al. RAS mutations are the predominant molecular alteration in poorly differentiated thyroid carcinomas and bear prognostic impact. J Clin Endocrinol Metab 2009;94:4735–4741.
13. Costa AM, Herrero A, Fresno MF, et al. BRAF mutation associated with other genetic events identifies a subset of aggressive papillary thyroid carcinoma. Clin Endocrinol (Oxf) 2008;68:618–634.
14. Ricarte-Filho JC, Ryder M, Chitale DA, et al. Mutational profile of advanced primary and metastatic radioactive iodine-refractory thyroid cancers reveals distinct pathogenetic roles for BRAF, PIK3CA, and AKT1. Cancer Res 2009;69:4885–4893.

15. McKinzie PB, Parsons BL. Detection of rare K-ras codon 12 mutations using allele-specific competitive blocker PCR. Mutat Res 2002;517:209–220.
16. McKinzie PB, Parsons BL. Accumulation of K-Ras codon 12 mutations in the F344 rat distal colon following azoxymethane exposure. Environ Mol Mutagen 2011;52:409–418.
17. Parsons BL, Marchant-Miros KE, Delongchamp RR, et al. ACB-PCR quantification of K-RAS codon 12 GAT and GTT mutant fraction in colon tumor and non-tumor tissue. Cancer Invest 2010;28:364–375.
18. Verkler TL, Delongchamp RR, Miller BJ, Webb PJ, Howard PC, Parsons BL. Simulated solar light-induced p53 mutagenesis in SKH-1 mouse skin: A dose-response assessment. Mol Carcinog 2008;47:599–607.
19. Wang Y, Meng F, Arlt VM, Mei N, Chen T, Parsons BL. Aristolochic acid-induced carcinogenesis examined by ACB-PCR quantification of H-Ras and K-Ras mutant fraction. Mutagenesis 2011;26:619–628.
20. Al-Mulla F, MacKenzie EM. Differences in in vitro invasive capacity induced by differences in Ki-Ras protein mutations. J Pathol 2001;195:549–556.
21. Al-Mulla F, Milner-White EJ, Going JJ, Birnie GD. Structural differences between valine-12 and aspartate-12 Ras proteins may modify carcinoma aggression. J Pathol 1999;187:433–438.
22. Hiltzik D, Carlson DL, Tuttle RM, et al. Poorly differentiated thyroid carcinomas defined on the basis of mitosis and necrosis: A clinicopathologic study of 58 patients. Cancer 2006;106:1286–1295.
23. Rivera M, Ghossein RA, Schoder H, Gomez D, Larson SM, Tuttle RM. Histopathologic characterization of radioactive iodine-refractory fluorodeoxyglucose-positron emission tomography-positive thyroid carcinoma. Cancer 2008;113:48–56.
24. Arcila ME, Oxnard GR, Nafa K, et al. Rebiopsy of lung cancer patients with acquired resistance to EGFR inhibitors and enhanced detection of the T790M mutation using a locked nucleic acid-based assay. Clin Cancer Res 2011;17:1169–1180.
25. Marchetti A, Milella M, Felicioni L, et al. Clinical implications of KRAS mutations in lung cancer patients treated with tyrosine kinase inhibitors: An important role for mutations in minor clones. Neoplasia 2009;11:1084–1092.
26. Molinari F, Felicioni L, Buscarino M, et al. Increased detection sensitivity for KRAS mutations enhances the prediction of anti-EGFR monoclonal antibody resistance in metastatic colorectal cancer. Clin Cancer Res 2011;17:4901–4914.
27. Landriscina M, Pannone G, Piscazzi A, et al. Epidermal growth factor receptor 1 expression is upregulated in undifferentiated thyroid carcinomas in humans. Thyroid 2011;21:1227–1234.
28. Pennell NA, Daniels GH, Haddad RI, et al. A phase II study of gefitinib in patients with advanced thyroid cancer. Thyroid 2008;18:317–323.
29. Myers MB, Wang W, McKim KL, Parsons BL. Hotspot oncomutation: Implications for personalized cancer treatment. Expert Reviews Molecular Diagnostics 2012;12:603–620.
30. Carnahan J, Beltran PJ, Babij C, et al. Selective and potent Raf inhibitors paradoxically stimulate normal cell proliferation and tumor growth. Mol Cancer Ther 2010;9:2399–2410.
31. Hatzivassiliou G, Song K, Yen I, et al. RAF inhibitors prime wild-type RAF to activate the MAPK pathway and enhance growth. Nature 2010;464:431–435.
32. Heidorn SJ, Milagre C, Whittaker S, et al. Kinase-dead BRAF and oncogenic RAS cooperate to drive tumor progression through CRAF. Cell 2010;140:209–221.
33. Poulikakos PI, Zhang C, Bollag G, Shokat KM, Rosen N. RAF inhibitors transactivate RAF dimers and ERK signalling in cells with wild-type BRAF. Nature 2010;464:427–430.
34. Arnault JP, Mateus C, Escudier B, et al. Skin tumors induced by sorafenib; paradoxic RAS-RAF pathway activation and oncogenic mutations of HRAS, TP53, and TGFBR1. Clin Cancer Res 2012;18:263–272.
35. Oberholzer PA, Kee D, Dziunycz P, et al. RAS mutations are associated with the development of cutaneous squamous cell tumors in patients treated with RAF inhibitors. J Clin Oncol 2012;30:316–321.
36. Su F, Viros A, Milagre C, et al. RAS mutations in cutaneous squamous-cell carcinomas in patients treated with BRAF inhibitors. N Engl J Med 2012;366:207–215.